Soft Matter

ARTICLE TYPE

Cite this: DOI: 00.0000/xxxxxxxxxx

Grafting density induced reentrant disorder-order-disorder transition in planar di-block copolymer brushes

Barbara Capone,*[a‡] Christos N. Likos,[b] and Ivan Coluzza[c]

Received Date
Accepted Date

DOI: 00.0000/xxxxxxxxxx

By means of multiscale molecular simulation, we show that solvophilic-solvophobic *AB* diblock copolymer brushes in the semi-dilute regime present a re-entrant disorder/order/disorder transition. The latter is fully controllable through two parameters: the grafting density and the solvophobic to solvophilic ratio of the tethered macromolecules. Upon increasing density, chains first aggregate into patches, then further order into a crystalline phase and finally melt into a disordered phase. We demonstrate that the order/disorder transition can be explained through the peculiar properties of the aggregates: upon increasing density, the aggregation number grows as expected. On the contrary their projection on the plane shrinks, thus melting the emergent ordered phase. Such a density dependent shrinkage, seen for the first time as the cause to an order/disorder phase transition, is as a consequence of the entropic/enthalpic competition that characterises the hierarchical self-assembly of the brush.

Polymer brushes are a class of polymeric systems made of macromolecules grafted on one end to a substrate or an interface[1]. The geometry of the grafting substrate and the nature of the grafted macromolecules give rise to a plethora of possible self-organising scenarios[2,3]. Simple homopolymeric brushes (*i.e.*, brushes made by homopolymers tethered to a substrate) and their properties have been extensively investigated both theoretically[4–10] and experimentally[11–14], corroborating the validity of scaling theories that predicted the dependence of brush height on both grafting density and solvent quality[2,3]. A considerably more complex scenario results by altering the local chemical composition of the tethered macromolecules. For example, by grafting *AB* solvophilic/solvophobic diblock copolymers onto substrates of various geometries, it is possible to exploit the rich morphology presented by such macromolecules in solution, to obtain complex coating patterns[13,15–19] arising from the competition between the entropic steric repulsion among the solvophilic regions of the grafted chains, and the effective enthalpic attraction in solvophobic regions. *AB* solvophilic/solvophobic diblock copolymer brushes are particular class of grafted macromolecular assembly, known to present a very complex self-aggregating scenario[13,16–19] arising from the competition between the entropic steric repulsion among the grafted chains, and the effective enthalpic attraction in solvophobic regions. Applications of diblock copolymer brushes range from template surface for mesoporous materials[20], to patterned surfaces[16], and to tissue engineering[21]. The versatility of diblock copolymer brushes attracted for almost three decades the attention of scientists from diverse sectors[15]. Nevertheless, the prediction of their assembly behaviour still presents a challenging problem. Self-consistent field theory has offered a very powerful tool for the prediction of the behaviour of such brushes for grafting densities starting from the melt, down to the semi-dilute regime [16,22–24]. Here, fluctuations in density weaken the predictive power of mean-field based approaches, rendering computational methods as the main but not always exhaustive exploration tool due to the large number of parameter involved.

In this paper, we focus on the self-assembly properties of *AB* diblock copolymer brushes, made of *A*-solvophilic heads grafted on a entropically repulsive planar surface, and of *B*-solvophobic ends exposed to the solvent, in the semi-dilute regime. Starting from a dilute system we establish, upon increasing grafting density, the emergence of patches on the surface, the ordering of such patches into a crystalline phase and in particular an unexpected re-entrant order-disorder phase transition.

The equilibrium phase diagram of diblock copolymer brushes generically depends on two parameters that balance the weight of the entropy/enthalpy contributions. The first is the fraction α of solvophobic monomers per grafted chain, while the second is the ratio σ/σ^* between the surface grafting density σ and the

[a] *Science Department, University of Roma Tre, Via della Vasca Navale 84, 00146, Rome, Italy; E-mail: barbara.capone@uniroma3.it*
[b] *Faculty of Physics, University of Vienna, Boltzmanngasse 5, A-1090 Vienna, Austria.*
[c] *Center for Cooperative Research in Biomaterials (CIC biomaGUNE), Basque Research and Technology Alliance (BRTA), Paseo de Miramon 182, 20014, Donostia San Sebastián, Spain.*

† Electronic Supplementary Information (ESI) available: See DOI: 00.0000/00000000.

overlap $\sigma^* = (\pi R_g^2)^{-1}$ of the same, *i.e.*, the density at which two neighbouring grafted chains of length L and radius of gyration $R_g \sim L^v$ would on average overlap. The resulting $(\sigma/\sigma^*, \alpha)$-phase diagram can be broadly divided in: an entropy-dominated region, where the steric repulsions between the grafted chains dictate the global behaviour of the system, and an enthalpy dominated one where the solvophobic ends start to interact[16,24]. The entropy dominated phase of the $(\sigma/\sigma^*, \alpha)$-phase diagram, is a region in which - on average - the terminal ends of the grafted diblocks do not interact. The grafted polymeric chains fluctuate similarly to homopolymeric chains and no significant aggregation is seen on the grafted substrate. As the $(\sigma/\sigma^*, \alpha)$ combination allows for a non zero probability of binding of the terminal solvophobic ends, we enter, upon increasing σ/σ^* or α, the enthalpy-dominated region. Here, the density of attractive monomers in solution is sufficiently high, and the latter aggregate and form clusters (patches), that then fluctuate on a "soft substrate" of solvophilic heads. The transition from the entropy to the enthalpy dominated phase is where the self-assembly process takes place, and it lies in the semi-dilute regime. The exploration of such a density region is challenging computationally, as all equilibrium properties are strongly affected by spatial inhomogeneity, local density fluctuations, and finite size effects[25], thus requiring the analysis of extremely large systems. To this end we make use of the Soft-Effective-Segment (SES) coarse-graining methodology[26,27], an approach that allows to explore large systems, made of thousands of chains each consisting – in its full monomer representation – of thousands of monomers. SES has been already proven to be able to quantitatively characterise equilibrium properties of macromolecular assemblies of the most diversified geometrical and chemical composition, with continuous possibility of backtracking the coarse grained results onto a well defined underlying monomer described system[27–30]. Within SES, groups of monomers are represented by means of first principles effective potentials, retaining all information on temperature, solvent quality and many body contributions[26,27,31].

We here consider brushes made of diblock copolymer chains of length $L = 10^6$ monomers, with a percentage α of solvophobic monomers spanning the range from 30% up to 80%. We investigate a wide range of grafting ratios σ/σ^* from 1 up to 26. The SES interaction potentials between all of the monomer species are reported in the Supporting Information (SI). It is important to stress that the range is within the semi-dilute regime and we do not reach the melt where we expect a lamellar phase with a solvophobic layer standing on a solvophilic one. In the semi-dilute regime, the SES coarse graining procedure has been shown to be able to quantitatively reproduce properties of the corresponding microscopic system [27,28,32–34] (see Simulation Methods in SI for details). All distances are reported in units of the bond length b of the underlying full monomer representation, while free energies (effective interactions between beads) are in units of k_BT; temperatures are expressed in reduced units, where room temperature corresponds to $T = 1$. To speedup equilibration and sampling, we employ the Virtual Move Parallel Tempering (VMPT) [35] method, which in our previous studies on hompolymer brushes, has proven to be extremely effective in sampling the brush profiles[9,10]. A typical VMPT simulation is performed at different reduced temperatures (4.0, 3.5, 3.0, 2.7, 2.5, 2.2, 2.0, 1.5, 1.2, 1.1, 1.0, 0.8, 0.5, 0.3, 0.2, 0.1), we run the simulation in parallel at higher additional temperatures to help overcome barriers in the phase space. However, we are only interested in the behaviour of the system at the reduced temperature $T = 1$ where the SES potential are valid. We have considered both the scenarios where the anchoring point is fixed or mobile on the grafted surface, without observing a significant difference in the behaviour of the copolymer brush, as previously reported for the case of homopolymeric brushes[9,10]. The reason is that the chains are long and well above the scaling limit which is imposed by SES representation. By collecting all our simulations, we can sketch a phase diagram for the system as a function of the $(\sigma/\sigma^*, \alpha)$ combination, as drawn in figure 1.

The green area in panel (b) of Fig. 1 shows the $(\alpha, \sigma/\sigma^*)$ region where there is no significant inter-molecular interaction between the solvophobic tails of the different macromolecules (*gas*-phase). The brush remains in an "open" configuration. Such a phase is characterised by a carpet of isolated collapsed tails monomers, each anchored to the surface via its solvophilic head (see Fig. 2a). The σ/σ^* boundary of the gas phase shrinks with increasing α indicating that aggregates forms only when the density of attractive monomers is over a minimum value.

When the local monomeric density of the solvophobic terminal ends reaches a threshold, tails belonging to different chains aggregate into functionalised regions, or patches. As the latter are formed, they are expelled from the solvophilic region of the brush and exposed to the solvent. Each aggregate takes the shape of a "pinned micelle"[16,24] where the core region is formed by the clustered attractive tails, and a corona tethered to the surface is formed by the corresponding self-avoiding heads (see Fig. 2c). The patches fluctuate, on average, around an equilibrium planar configuration parallel to the grafted substrate.

The region $\alpha \in [0.5, 0.7]$ shows for $\sigma/\sigma^* \in [7.0, 13.0]$ (red squares in Fig. 1b) the emergence of an ordered 2D crystalline phase, or *solid*-phase (see Fig. 2b). This phase is suppressed when the grafting density is further increased: patches lose their 2D order and fluctuate in both parallel and orthogonal directions on a plane parallel to the grafting surface, and a *liquid*-phase arises from the crystalline region (see Fig. 2d). It is important to stress that for $\alpha = 0.4$ the system goes directly form the *gas*- to the *liquid*-phase, while for $\alpha = 0.8$ we only observe the *liquid*-phase.

For clarity reasons, we here focus on the description of the re-entrant transition for the $\alpha = 0.6$ system; however the phenomenology is valid for all the all of the asymmetry ratios we analysed $\alpha \in [0.4, 0.8]$ and all grafting densities, as we report in detail in the SI. The self-assembly behaviour involves the collapse of multiple chains into the pinned micelle configuration. We hence employed a cluster analysis algorithm (see description in SI) to characterise size, height distribution $\phi(z)$ of the patches with respect to the grafting surface, and the relative arrangement of the aggregates through their pair distribution function $g(r)$ and the distribution $\Pi(\alpha_p)$ of the α_p angles between neighbouring patches (see definitions in SI).

The cluster analysis in the *gas*-phase indicates the coexistence of small intermolecular and many intramolecular clusters (see the black histogram in Fig. 3). In this case, the $g(r)$ between patches does not present any sign of structure and the angular distribution $\Pi(\alpha_p)$ between neighbouring patches is featureless (see green inset in Fig. 1 and in the SI the Fig. S6 and Fig. S9).

In the *solid*-phase, all grafted chains participate to the formation of patches of finite size, that align along preferential directions with respect to the grafting plane. A strong signature of structure is seen in both the radial distribution function between aggregates, and the average angle distribution between neighbouring patches, that sharply distributes around 60° as shown in the red inset of Fig. 1 (and in Fig. S10 in the SI). The size of the unit cell of the assembled crystals is controlled by the radius R_{corona}

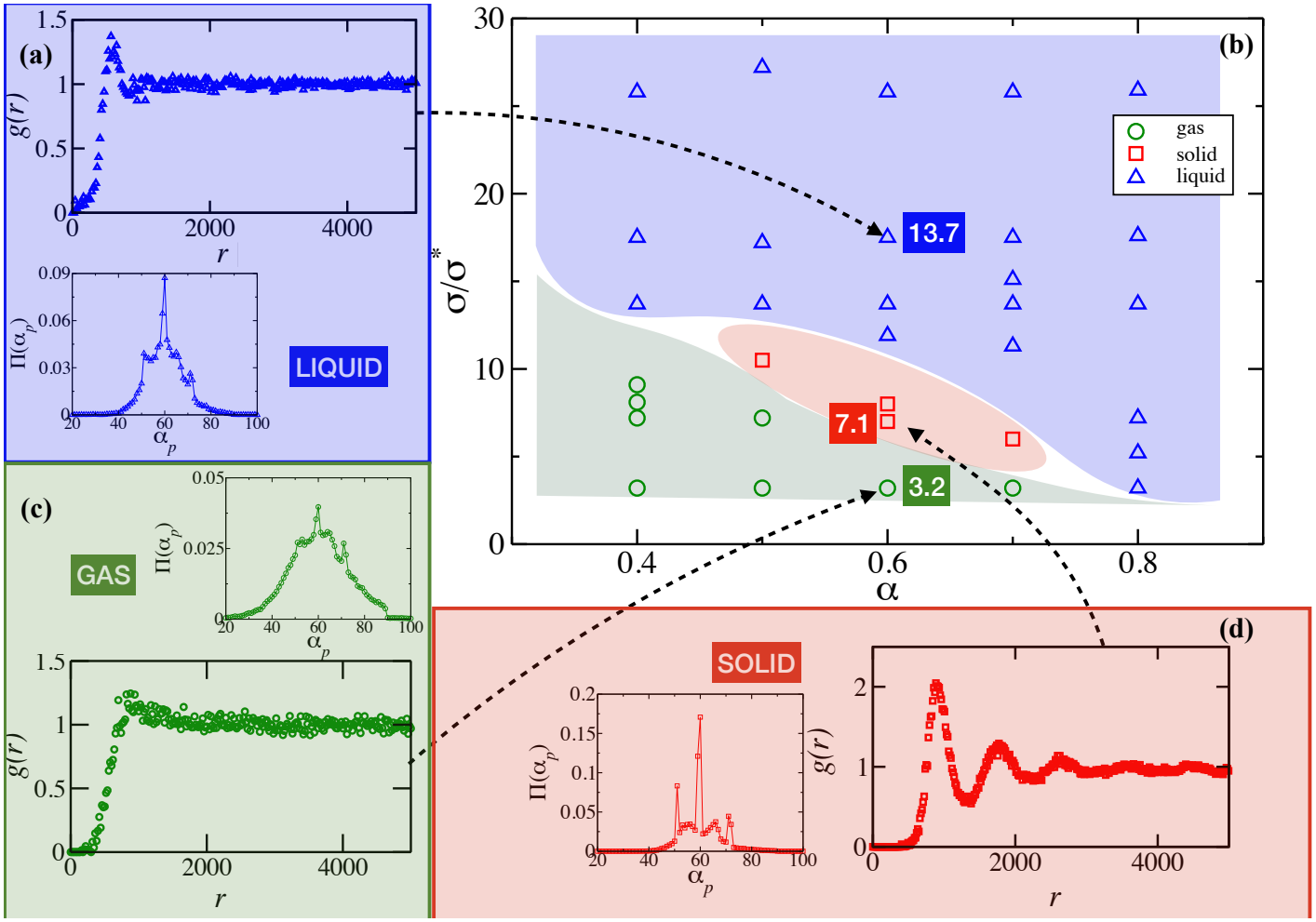

Fig. 1 Phase Diagram for the gas-solid-liquid transition as a function of the asymmetry ratio α and the density ratio σ/σ^* in panel (b). It is possible to see the appearance of the solid phase as a re-entrant phase (in red - panel (d)) squeezed between the gas (green - panel (c)) and liquid (blue - panel (a)) phases. In the insets we follow the transition along the $\alpha = 0.6$ line. In every inset we show the distribution $\Pi(\alpha_p)$ of the angle α_p between pairs of first neighbouring patches (see SI), and the radial distribution $g(r)$ of the solvophobic monomers, where r is the distance between the centres of masses of the aggregates expressed in units of the persistence length b of the underlying microscopic representation.

(see Fig. S4 in the SI). The latter is defined as the average radius of the 2D projection on the grafted surface of the pinned micelles' coronas. By normalising the radial distances by R_{corona}, the first peak of the crystalline $g(r)$ re-scales to unity (see inset of Fig. S7 in the SI). Furthermore, the disorder-order transition between the *gas* and *solid*- phases distributes the patches at a fixed height from the underlying surface (see Fig. S12 in the SI). As the grafting density is further increased, the patches start oscillating both in the z-direction (see Fig. S12 in the SI) as well as in the xy-plane. Order gets lost and we see the appearance of the *liquid*-phase.

In the blue inset of Fig. 1 (and in Fig. S8 in the SI) we show the 2D radial distribution function computed on the projection on the xy plane of the coordinates of the centre of mass of the patches, for the high overlapping densities $\sigma/\sigma^* > 13$. The $g(r)$ shows short-range oscillations typical of a fluid phase, where translational order decays rapidly with the intraparticle distance. The angular distribution $\Pi(\alpha_p)$ in the blue inset of Fig. 1 (and in Fig. S11 in SI) also shows a strong loss of order: the sharp peak around 60° appears smoothed with respect to the solid one, resembling more and more to the *gas*-phase one in Fig. S9. We will thus interpret all of the phases characterised by such a combination of $g(r)$ and $\Pi(\alpha_p)$, as *liquid*-phases.

In Fig. 3 we show the cluster size distribution for the three phases. The *gas*-phase presents the coexistence of single chain intramolecular clusters with small intermolecular clusters. Aggregates formed in the solid phase are quite monodisperse, with a cluster size distribution that is sharply peaked. As soon as density is increased, and the crystal melts in favour of a *liquid*-phase. The average cluster size grows, and the width of the cluster distribution spreads. On the other hand, R_{corona} decreases *e.g.*, by $\sim 10\%$ for the $\alpha = 0.6$ case, passing from $762b$ (bond lengths) in the crystal phase ($\sigma/\sigma^* = 7.1$) to $483b$ deep in the liquid phase ($\sigma/\sigma^* = 25.8$). The reduction in the coronae of the pinned micelles can also be appreciated by comparing the solid and liquid $g(r)$ (see in Fig. S7 and Fig. S8 in the SI). The position of the first peak - in microscopic units - is centred around 1000[b] for the solid case, while the liquid phase shows an average distance between nearest neighbours of about $500 - 600$[b].

To understand such an apparently counter-intuitive behaviour, we analyse the scaling of the average brush height as a function of density. Reminiscent of the scaling of a homopolymer brush, we observe that, as grafting density is increased, the brush as a whole is stretched, and patches are clearly expelled outwards. Reaching the liquid phase, the aggregates float on a carpet of fully stretched solvophilic chains, see Fig. 4. To formalise the correlation between the stretching of the brush and the shrinkage of the corona radius, we performed a scaling analysis (see SI) where R_{corona} is obtained by minimizing the total free energy of the pinned micelles for every density. Taking into account the free energy contributions of

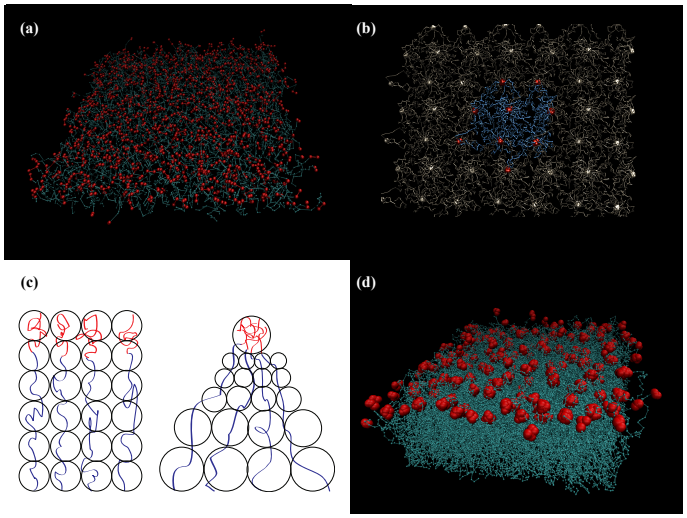

Fig. 2 Snapshots of the typical diblock copolymer brush conformations for the three different phases (a) gas, (b) solid (d) liquid. (c), left: sketch of the gas phase: the end of the chains are not cross- interacting and cover uniformly the surface of the brush. (c), right: sketch of the pinned micelles in the aggregated phases (solid and liquid). (d) snapshot of the re-entrant liquid. Upon increasing the ratio σ/σ^* the aggregates melt the 2D-crystalline pattern shown in (b). In all snapshots, red are the solvophobic monomers, cyan are the solvophilic ones.

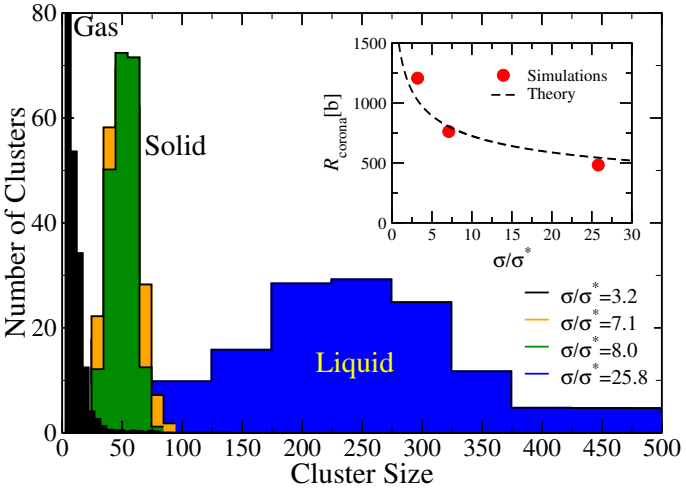

Fig. 3 Number of clusters as function of their size for the *gas*, *solid*, and *liquid* phases for the $\alpha = 0.6$ system. The corona radius of gyration R_{corona} of the clusters in three phases are respectively: 1207, 762 and 483 in units of bond length. The inset shows the behaviour of R_{corona} obtained in simulations as a function of the grafting density σ. We show in the SI (see eq. S9 and Figure S3) that such a behaviour can be predicted and explained by using scaling theories. The line between the points is the result of the scaling theory; the errors on every simulation point is smaller than the symbol. To stress the dependence of the phase on the cluster size, we show two different values of σ/σ^* ($\sigma/\sigma^* = 7.1, 8.0$), characterised by a very similar average number of clusters, and both belonging to the solid phase.

both the packing of the monomers in the patch, and the stretching of the chains belonging to the coronae, scaling theories (see dedicated section in SI) confirm that R_{corona} decreases with as σ/σ^* grows, as shown in the inset of Fig. 3. Hence, the re-entrant behaviour is the result of two concurring effects: the reduction of the R_{corona} and the loss of the 2D confinement (double peaks in Fig. S12 int he SI) reminiscent of the phase observed in core-softned colloids by Osterman *et al.*[36].

In this work we analysed the properties of solvophilic/solvophobic diblock copolymer brushes in the semi-dilute regime. The computational investigation was made through a coarse grained approach known as the soft-effective-segment methodology[28,32], that allows to regroup thousands of monomers into an effective potential, while retaining quantitative predictions on equilibrium properties of the system. We analysed the self-assembling properties of substrates grafted by thousands of polymers each made of millions of monomers.

We mapped the configurational space of the brush into the phase space of the $\sigma/\sigma^*, \alpha$ parameters that fully control the self-assembling properties of brush. We identified the presence of a re-entrant disorder/order/disorder transition in the $\sigma/\sigma^*, \alpha$ phase space. The ordered phase corresponds to a 2D crystalline array of patches formed by the assembled solvophobic tails of the polymers. We show how to control the crystalline order by changing the $\sigma/\sigma^*, \alpha$ parameters. Hence, producing a tunable crystalline surface with many applications for patterning and templating the growth of materials from the surface. The second key observation that we performed concerns the mechanism for the re-entrant transition. We have demonstrated, both computationally and theoretically, that the increase in the grafting density stretches the pinned micelles outwards reducing their 2D effective radius. To the best of our knowledge such a mechanism has never been observed before and represents a novel physical approach to control the ordering of a 2D system. In particular the ordered phase has not been experimentally observed yet. The results presented in Fig. 1 offers a precise map to guide potential new experiments.

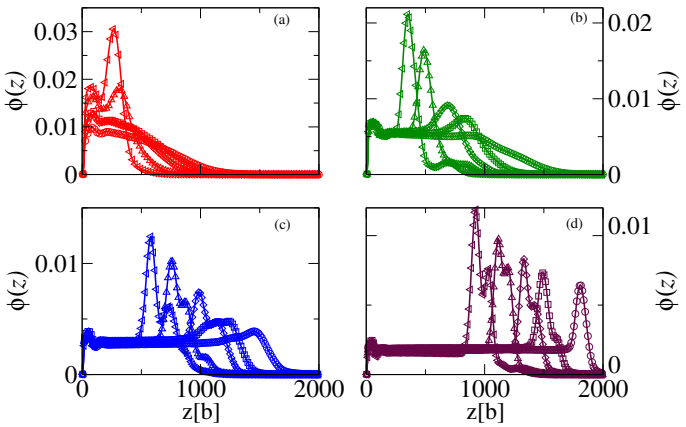

Fig. 4 Height distribution for the brushes with asymmetry ratio $\alpha \in [0.4, 0.8]$ and $\sigma/\sigma^* \in [3.2, 25.8]$. Same colour indicates same grafting density: (a) red for $\sigma = 3.2\sigma^*$; (b) green for $\sigma = 13.7\sigma^*$; (c) blue for $\sigma = 23\sigma^*$; and (d) maroon for $\sigma = 25.8\sigma^*$. Symbols indicate α-values: circles for $\alpha = 0.4$, squares for $\alpha = 0.5$, diamonds for $\alpha = 0.6$, triangles up for $\alpha = 0.7$ and triangles left for $\alpha = 0.8$.

Acknowledgements

All simulations presented in this paper were carried out on the Vienna Scientific Cluster (VSC). BC acknowledges funding from the Marie

Curie Individual Fellowship, project ID 751255 and the Grant of Excellence Departments, MIUR-Italy (ARTICOLO 1, COMMI 314 - 337 LEGGE 232/2016). IC acknowledge support from the Austrian Science Fund (FWF) project 26253-N27. I.C. gratefully acknowledges support from the Ministerio de Economià y Competitividad (MINECO) (FIS2017-89471-R). This work was performed under the Maria de Maeztu Units of Excellence Program from the Spanish State Research Agency âĂŞ Grant No. MDM-2017-0720. This research was supported by Programa Red Guipuzcoana de Ciencia, TecnologÃ■a e InformaciÃşn 2019-CIEN-000051-01. We acknowledge support from try BIKAINTEK program (grant No. 008-B1/2020). The author(s) would like to acknowledge the contribution of the COST Action CA17139.

Notes and references

1 S. T. Milner, *Science*, 1991, **251**, 905–914.
2 S. Alexander, *J. Phys.*, 1977, **38**, 983–987.
3 P. G. de Gennes, *Macromolecules*, 1980, **13**, 1069–1075.
4 G. S. Grest, *Macromolecules*, 1994, **27**, 418–426.
5 R. R. Netz and M. Schick, *Macromolecules*, 1998, **31**, 5105–5122.
6 C. Yeung, K. Huang, D. Jasnow and A. C. Balazs, *Colloids Surfaces A Physicochem. Eng. Asp.*, 1994, **86**, 111–123.
7 P. Lai and K. Binder, *J. Chem. Phys.*, 1992, **97**, 586–595.
8 P. Lai and K. Binder, *J. Chem. Phys.*, 1991, **95**, 9288–9299.
9 I. Coluzza and J.-P. Hansen, *Phys. Rev. Lett.*, 2008, **100**, 016104.
10 I. Coluzza, B. Capone and J.-P. Hansen, *Soft Matter*, 2011, **7**, 5255–5259.
11 P. Auroy, L. Auvray and L. Léger, *Phys. Rev. Lett.*, 1991, **66**, 719–722.
12 A. Halperin, M. Tirrell and T. P. Lodge, *Macromol. Synth. Order Adv. Prop.*, 1992, **100**, year.
13 B. Zhao and W. J. Brittain, *Prog. Polym. Sci.*, 2000, **25**, 677–710.
14 R. R. Netz and D. Andelman, *Phys. Rep.*, 2003, **380**, 1–95.
15 O. Azzaroni, *J. Polym. Sci. Part A Polym. Chem.*, 2012, **50**, 3225–3258.
16 E. B. Zhulina, C. Singh and A. C. Balazs, *Macromolecules*, 1996, **29**, 8254–8259.
17 W. Senaratne, L. Andruzzi and C. K. Ober, *Biomacromolecules*, 2005, **6**, 2427–2448.
18 R. Barbey, L. Lavanant, D. Paripovic, N. Schüwer, C. Sugnaux, S. Tugulu and H.-A. Klok, *Chem. Rev.*, 2009, **109**, 5437–5527.
19 M. Urban, M. A. C. Stuart, W. T. S. Huck, F. Winnik, M. Müller, S. Zauscher, V. V. Tsukruk, G. B. Sukhorukov, I. Luzinov, C. Ober, J. Genzer, I. Szleifer, M. Stamm and S. Minko, *Nat. Mater.*, 2010, **9**, 101–113.
20 G. J. Soler-Illia and O. Azzaroni, *Chem. Soc. Rev.*, 2011, **40**, 1107–1150.
21 R. Singhvi, A. Kumar, G. P. Lopez, G. N. Stephanopoulos, D. I. Wang, G. M. Whitesides and D. E. Ingber, *Science*, 1994, **264**, 696–698.
22 R. M. Choueiri, E. Galati, H. Thérien-Aubin, A. Klinkova, E. M. Larin, A. Querejeta-Fernández, L. Han, H. L. Xin, O. Gang, E. B. Zhulina, M. Rubinstein and E. Kumacheva, *Nature*, 2016, **538**, 79–83.
23 E. Zhulina, Y. Lyatskaya and T. Birshtein, *Polymer (Guildf).*, 1992, **33**, 332–342.
24 E. B. Zhulina, C. Singh and A. C. Balazs, *Macromolecules*, 1996, **29**, 6338–6348.
25 P. G. de Gennes and T. A. Witten, *Phys. Today*, 1980.
26 B. Capone, I. Coluzza, R. Blaak, F. L. Verso and C. N. Likos, *New J. Phys.*, 2013, **15**, 095002.
27 B. Capone, I. Coluzza and J.-P. Hansen, *J. Phys. Condens. Matter*, 2011, **23**, 194102.
28 B. Capone, J.-P. Hansen and I. Coluzza, *Soft Matter*, 2010, **6**, 6075.
29 A. Narros, A. J. Moreno and C. N. Likos, *Macromolecules*, 2013, **46**, 3654–3668.
30 I. Coluzza, P. D. J. van Oostrum, B. Capone, E. Reimhult and C. Dellago, *Phys. Rev. Lett.*, 2013, **110**, 075501.
31 V. Krakoviack, J. P. Hansen and A. A. Louis, *Phys. Rev. E*, 2003, **67**, 41801.
32 C. Pierleoni, B. Capone and J.-P. Hansen, *J. Chem. Phys.*, 2007, **127**, 171102.
33 I. Coluzza, B. Capone and J.-P. J.-P. Hansen, *Soft Matter*, 2011, **7**, 5255.
34 A. Narros, C. N. Likos, A. J. Moreno and B. Capone, *Soft Matter*, 2014, **10**, 9601–9614.
35 I. Coluzza and D. Frenkel, *ChemPhysChem*, 2005, **6**, 1779–1783.
36 N. Osterman, D. Babič, I. Poberaj, J. Dobnikar and P. Ziherl, *Phys. Rev. Lett.*, 2007, **99**, 248301.